Influence of the rare earth (R) element in Ru-supported RScSi electride-like intermetallic catalysts for ammonia synthesis at low pressure: insight into NH3 formation mechanism

Charlotte Croisé, Khaled Alabd, Sophie Tencé, Etienne Gaudin, Antoine Villesuzanne, Xavier Courtois, Nicolas Bion, Fabien Can

ChemCatChem

Research Article
doi.org/10.1002/cctc.202201172

Chemistry Europe
European Chemical Societies Publishing

www.chemcatchem.org

Special Collection

Influence of the Rare Earth (*R*) Element in Ru-supported *R*ScSi Electride-like Intermetallic Catalysts for Ammonia Synthesis at Low Pressure: Insight into NH_3 Formation Mechanism

Charlotte Croisé,[a] Khaled Alabd,[b] Sophie Tencé,[b] Etienne Gaudin,[b] Antoine Villesuzanne,[b] Xavier Courtois,[a] Nicolas Bion,[a] and Fabien Can*[a]

This study investigates the influence of the rare-earth (*R*) element in Ru/*R*ScSi electride-like intermetallic catalysts for ammonia synthesis under mild conditions (300–450 °C; 1–5 bar). All materials present poor specific surface area and the grain size impacts the ammonia yield. The catalytic performances follow the La to Gd lanthanides series ($Ru_{1.7}$/LaScSi = $Ru_{1.7}$/CeScSi = $Ru_{1.7}$/PrScSi > $Ru_{1.7}$/NdScSi > $Ru_{1.5}$/SmScSi > $Ru_{1.3}$/GdScSi) and appear correlated with the formation of the hydride phase. $Ru_{1.7}$/CeScSi shows remarkable catalytic activity under moderate condition (0.58 $mmol_{NH3}$/h/g at 300 °C, 1 bar) associated with its reversible hydrogen storage–release properties. It is evidenced that *R*ScSi materials assist the N_2 dissociation in agreement with their electride character and that the hydrogen for NH_3 formation mainly comes from gaseous hydrogen and not primarily from the hydride phase. It is suggested that NH_X formation could be the rate determining step rather than the N_2 cleavage over these catalysts.

Introduction

Ammonia synthesis represents a major worldwide challenge since ammonia is one of the most synthesized chemicals in the world, with a production reaching almost 180 million tons per year.[1] The production continues to rise every year due to the important demand in organic and inorganic chemistry, especially as nitrogen source in fertilizers for agricultural crops. In recent years, NH_3 was also envisaged to be used directly as fuel in the next generation of more efficient fuel cells that do not emit CO_2.[2] In addition, ammonia synthesis is a promising alternative way to store energy since NH_3 is easy to liquefy compared to H_2. Ammonia could become a hydrogen carrier with a high H storage capacity and a higher volumetric H density than liquid H_2.[3]

The Haber-Bosch process remains currently the main industrial technology for ammonia production thanks to the use of Fe-based catalysts. Although the reaction is exothermic ($N_2 + 3H_2 \rightarrow 2NH_3$; $\Delta H° = -92\ kJ\,mol^{-1}$), high temperatures (400–600 °C) are necessary for the process to be efficient because the trivalent bond of the N_2 molecule is highly refractory ($945\ kJ\,mol^{-1}$). To compensate for the low yields achieved at high temperatures, high pressures (200 bar) are also applied.[4] It results in high energy consumption (1–2% of the world's annual energy supply) and thus in emission of greenhouse gases. The improvement of the Haber-Bosch process involves the development of catalytic materials active in the cleavage of the N≡N bond by electron donation, commonly recognized as the rate-determining step of ammonia synthesis. Supported ruthenium (Ru) catalysts are claimed to be good candidates for NH_3 synthesis and the back-donation of electrons to N_2 can be promoted by addition of alkali or alkaline earth metals.[5] However, despite these improvements, the operating pressure of the Haber–Bosch process remains high and the Ru metal is subject to hydrogen poisoning that lowers the efficiency of the reaction. Therefore, more efficient catalysts for sustainable ammonia synthesis are still expected.

Important efforts have been made to develop new active materials: metals nitrides, LiH support or amide-based samples were recently claimed to enhance the ammonia synthesis rate.[6] Another promising solution is the use of electride materials whose electron-donating effect is expected to promote the N_2 dissociation. Electrides are crystals that contain excess electrons periodically located in crystallographic sites throughout the lattice.[7] These extra electrons play the role of anions. Such materials were known as unstable until Matsuishi *et al.* discovered in 2003 the first stable electride, $[Ca_{24}Al_{28}O_{64}]^{4+}(e^-)_4$,[8] that was successfully used in 2012 as an activator for the Ru-based

[a] C. Croisé, Dr. X. Courtois, Dr. N. Bion, Dr. F. Can
Institut de Chimie des Milieux et Matériaux de Poitiers (IC2MP)
Université de Poitiers, CNRS.
4 rue Michel Brunet
TSA 51106 86073 Poitiers Cedex 9 (France)
E-mail: fabien.can@univ-poitiers.fr
[b] K. Alabd, Dr. S. Tencé, Dr. E. Gaudin, Dr. A. Villesuzanne
Univ. Bordeaux, CNRS, Bordeaux INP, ICMCB, UMR 5026
F-33600 Pessac (France)

Supporting information for this article is available on the WWW under https://doi.org/10.1002/cctc.202201172

Special Collection *This publication is part of a Special Collection on "French Conference on Catalysis 2022". Please check the ChemCatChem https://chemistry-europe.onlinelibrary.wiley.com/doi/toc/10.1002/(ISSN)1867-3899.french-conference-catalysis-2022 homepage for more articles in the collection:*

catalysis for ammonia synthesis.[9] These results demonstrate the very attractive potential of this type of materials for ammonia synthesis under mild conditions. Since, several intermetallic silicides such as La(Co,Mn,Fe)Si,[10] LaRuSi,[11] LaNiSi[12] or Y_5Si_3[13] have been reported as active catalyst in NH_3 synthesis. Very recently, Wu *et al.* have demonstrated that the use of the electride-like intermetallic phase LaScSi combined with Ru enables to reach one of the highest reported production rate of ammonia at ambient pressure (4.8 mmol/g/h at 400 °C, compared to 0.2 mmol/g/h for Ru/CaO with the same experimental conditions and Ru loading, at 1.5 $_{wt}$%).[14]

The *RTX* intermetallics crystallizing in the CeScSi-structure type are usually composed of *R* = Y, La–Tm, Lu; *T* = Sc, Ti, Zr and *X* = Si, Ge, Sn, Sb[15] and can present a large capacity in hydrogen absorption. Indeed, their structure contains rare-earth tetrahedral voids [R_4] as well as mixed rare-earth/transition metal or Sc octahedral voids [R_2T_4], both suitable for hydrogen insertion. *RTX* compounds with rare earths such as lanthanum (La), cerium (Ce), neodymium (Nd) and gadolinium (Gd) have been identified as promising candidates for hydride formation. The hydride character is claimed to avoid the poisoning of ruthenium by adsorbed H species due to surface H^- ion mobility, that would play a major role in ammonia synthesis by providing a high catalyst durability for the Haber-Bosch process.[9,16] In particular, the hydrogenation properties of LaScSi, CeScSi, NdScSi, GdScGe or GdTiGe have been recently published.[17]

However, a systematic study of the impact of the rare earth element (*R*) in *R*ScSi ternary intermetallics for the catalytic Haber-Bosch synthesis is still lacking. In fact, Gong *et al.*[18] recently noted the great potential of rare earth-containing catalysts for more efficient ammonia synthesis. In addition, ammonia production at the laboratory scale is usually monitored under steady-state conditions of temperature, by ammonia trapping in a sulphuric acid solution and subsequent analysis by ion chromatography. As a result, it is not possible to obtain crucial information on the evolution of the materials activity during temperature rise and catalysts activation.

In this paper, we investigate the influence of the rare earth element (*R*=La, Ce, Pr, Nd, Sm, Gd) in Ru supported *R*ScSi electride-like catalysts for ammonia synthesis under mild conditions of pressure and temperature. A specific attention is made on low temperature activity (300 °C, 1–5 bar) and new insights into NH_3 formation mechanism are considered using N_2 isotopic exchange measurements and transient flow experiments.

Results and Discussion

Catalysts characterization

The comparison of the powder XRD patterns of the as-cast and annealed samples confirms the formation of the main phase *R*ScSi after annealing, with the presence of a few amount of the secondary phase Sc_5Si_3 (less than 4 $_{wt}$%). The SmScSi sample also has a small amount of Sm_5Si_3 (approx. 3 $_{wt}$%), and the GdScSi sample contains approximately 6 $_{wt}$% of $Gd_{2.45}Sc_{2.55}Si_3$ solid solution. All patterns were indexed with the tetragonal space group *I*4/*mmm* with unit cell parameters in agreement with previous published data (gathered in Table 1).[14,17]

The ruthenium loadings in the studied materials, obtained from ICP analysis, are between 1.3 $_{wt}$% and 1.7 $_{wt}$% (Table 2). The ruthenium particle sizes were determined by TEM-EDX analysis. Histograms of the size distributions of Ru particles show irregular morphology (Figure S1 in the Supplementary Information file, and also illustred in Figure 3A for $Ru_{1.4}$/LaScSi). The average Ru particles size, depending on the intermetallic formula, are estimated between 5 nm and 18 nm, as presented in Table 2.

The dispersion values are calculated from different models, as described in the experimental part, to cover the full range of particle sizes. The dispersion ranges from 7 to 25 % depending on the involved intermetallic support. Note that the particle size and dispersion values also depend on the Ru loading, as illustrated by the comparison of $Ru_{1.4}$/LaScSi and $Ru_{1.7}$/LaScSi

Table 1. Unit cell parameters from XRD data before and after catalytic tests at 400 °C (1, 3, and 5 bar) for different catalyst support, along with the phases found after the catalytic test.

intermetallic support	Cell parameters of the intermetallic phase before catalytic test	Phases found after catalytic test[a]	Cell parameters of the hydrides after catalytic test
LaScSi	a = 4.355(1) Å c = 16.031(1) Å	$LaScSiH_x$[b]	a = 4.273(1) Å c = 17.045(1) Å
CeScSi	a = 4.337(1) Å c = 15.794(1) Å	$CeScSiH_x$[c]	a = 4.246(1) Å c = 16.778(1) Å
PrScSi	a = 4.313(1) Å c = 15.690(1) Å	$PrScSiH_x$[c]	a = 4.251(1) Å c = 16.453(3) Å
NdScSi	a = 4.295(1) Å c = 15.685(1) Å	NdScSi (20 %) $NdScSiH_x$[d] (80 %)	a = 4.208(1) Å c = 16.576(2) Å
SmScSi	a = 4.262(1) Å c = 15.555(1) Å	SmScSi (47 %) $SmScSiH_x$[c] (53 %)	a = 4.174(1) Å c = 16.436(2) Å
GdScSi	a = 4.239(1) Å c = 15.467(1) Å	GdScSi	

[a]: this only includes main intermetallic pristine or hydride phases with an estimation of their relative proportion ($_{wt}$%), and does not include secondary phases like Sc_5Si_3 or CeO_2. [b]: x value lies between 1.2 and 1.5 based on hydrides characterized in [14] where $LaScSiH_{1.5}$ has the parameters a = 4.271 Å and c = 17.090 Å and $LaScSiH_{1.2}$ has the parameters a = 4.261 Å and c = 17.039 Å. [c]: the hydrides with these cell parameters were characterized for the first time. [d]: x is lower than 1.5 based on data from [17a,b] where $NdScSiH_{1.5}$ has the parameters a = 4.221 Å and c = 16.928 Å.

Table 2. Catalysts characterization.

	Ru loading [$_{wt}$%][a]	Particle size [nm][b]	Ru Dispersion hcp [%][c]	Ru Dispersion spherical [%][c]
$Ru_{1.4}$/LaScSi	1.4	5.6	22.5	25.1
$Ru_{1.7}$/LaScSi	1.7	13.0	11.0	10.2
$Ru_{1.7}$/CeScSi	1.7	11.5	12.1	11.6
$Ru_{1.7}$/PrScSi	1.7	15.5	9.5	8.6
$Ru_{1.7}$/NdScSi	1.7	9.0	14.7	14.8
$Ru_{1.5}$/SmScSi	1.5	18.1	8.4	7.3
$Ru_{1.3}$/GdScSi	1.3	17.5	8.6	7.6
$Ru_{2.1}$/MgO	2.1	1.8	53.4	73.9

[a]: the Ru content was determined by ICP-OES experiments. [b]: Particle size were determined by TEM analysis. [c]: dispersion was calculated assuming spherical metal particles or hexagonal close packed particles (*hcp*) model.

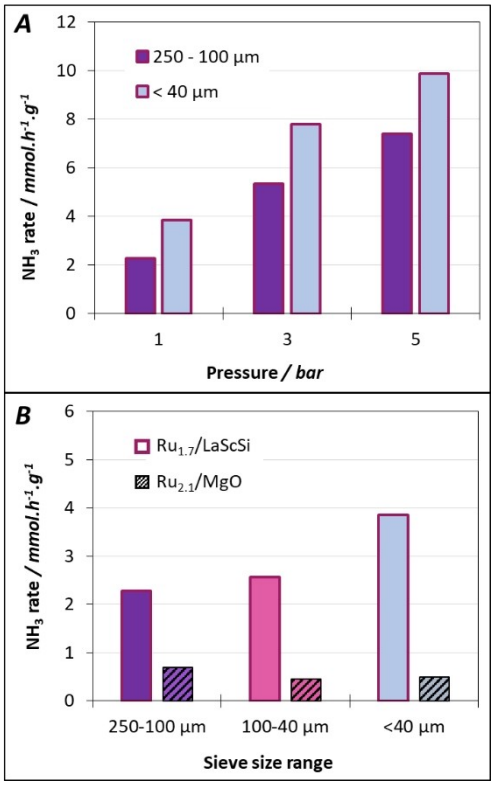

Figure 1. A: Impact of catalyst sieving on ammonia synthesis at 450 °C over $Ru_{1.7}$/LaScSi depending on pressure; B: Focus at 1 bar (450 °C) for $Ru_{1.7}$/LaScSi (□) and $Ru_{2.1}$/MgO (▨).

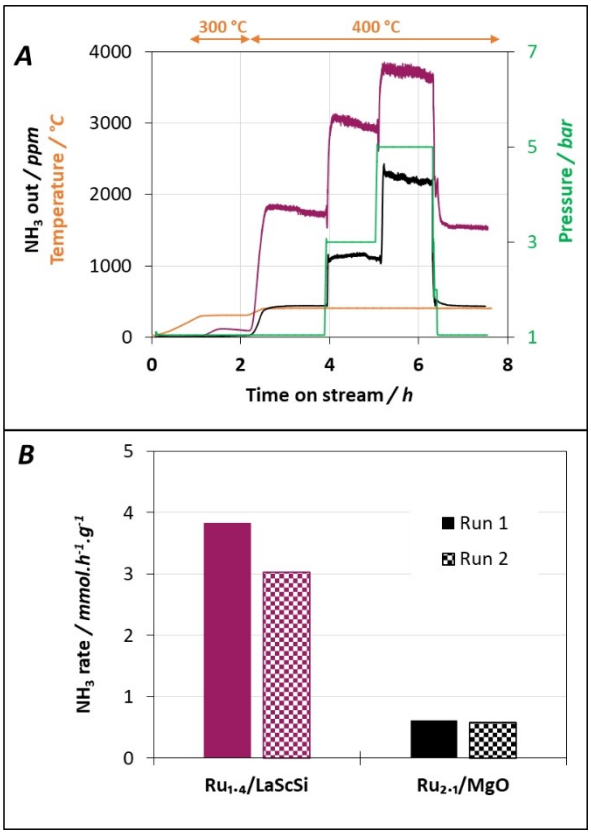

Figure 2. A: evolution of the ammonia production over $Ru_{1.7}$/LaScSi ((■) and $Ru_{2.1}$/MgO (■) depending on the temperature and pressure. B: Effect of number of runs on ammonia synthesis at 400 °C and 1 bar for 100–40 µm over $Ru_{1.4}$/LaScSi ((■) and $Ru_{2.1}$/MgO (■).

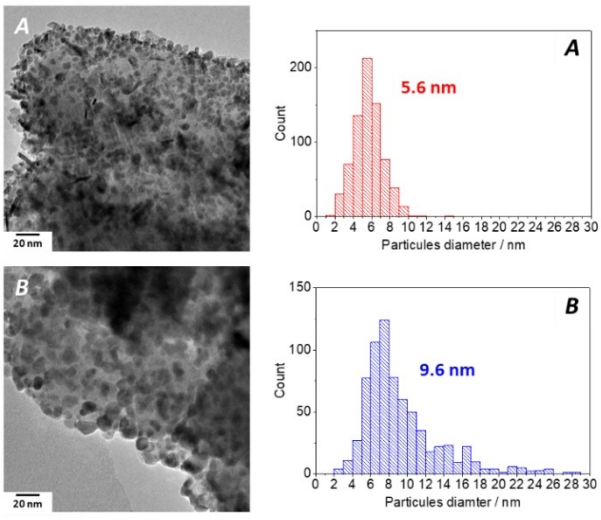

Figure 3. TEM images and particle size distribution of $Ru_{1.4}$/LaScSi (100–40 µm). A: Before catalytic test. B: After 2 catalytic runs at 400 °C up to 5 bar.

samples (Table 2). The effect of Ru particle size in NH_3 synthesis rate is discussed thereafter (Figure 4, Table 4).

Catalyzed ammonia synthesis

In a first set of preliminary tests, the effect of catalyst sieving and catalyst stability as a function of time on stream were investigated on the $Ru_{1.7}$/LaScSi intermetallic and compared to the $Ru_{2.1}$/MgO reference material. A study on the sintering of ruthenium particles was also performed on the $Ru_{1.4}$/LaScSi material.

Because of the extremely low porosity of intermetallic materials, the grain size of the samples should have a strong

Table 3. NH_3 emission */ppm* for 1 hour of NH_3 synthesis at 300 °C and 400 °C over Ru/*R*ScSi catalysts (100-40 μm) and N_2 equilibrium rate at 450 °C (from isotopic exchange measurements).

Temp. [°C]		1 bar	3 bar	5 bar	Return 1 bar	N_2 equilibrium rate at 450 °C, $R_q/10^{22}$ *at.g^{-1}.min^{-1}*[a]
400 °C	Thermodynamic	**3743**	**11066**	**18179**	**3743**	
	$Ru_{1.4}$/LaScSi	2560	4577	5421	2361	
	$Ru_{1.7}$/LaScSi	1710	2920	3650	1520	55.4
	$Ru_{1.7}$/CeScSi	1600	2930	3720	1505	50.1
	$Ru_{1.7}$/PrScSi	1559	2776	3584	1340	13.9
	$Ru_{1.7}$/NdScSi	1367	2334	2976	1210	1.52
	$Ru_{1.5}$/SmScSi	868	1275	1540	700	0.46
	$Ru_{1.3}$/GdScSi	420	910	1200	314	4.42
	$Ru_{2.1}$/MgO	420	1100	2170	434	0
300 °C	Thermodynamic	**17348**	**48769**	**76595**	**17348**	
	$Ru_{1.7}$/LaScSi	95	470	650	65	
	$Ru_{1.7}$/CeScSi	385	720	900	365	
	$Ru_{2.1}$/MgO	2	2	2	2	

[a]: determined from the slope of the m/z = 29 curve at the beginning of the isothermal $^{14}N_2/^{15}N_2$ nitrogen homomolecular isotopic exchange experiments.

Table 4. NH_3 production turn over frequency/*min^{-1}* in NH_3 synthesis at 300 °C and 400 °C over Ru/RScSi catalysts (100–40 μm, average TOF for 1 h measurement).

Temp. [°C]		1 bar	3 bars	5 bars	Return 1 bar
400 °C	$Ru_{1.4}$/LaScSi	2.0	3.6	4.3	1.9
	$Ru_{1.7}$/LaScSi	2.4	4.1	5.1	2.1
	$Ru_{1.7}$/CeScSi	1.9	3.5	4.4	1.8
	$Ru_{1.7}$/PrScSi	2.6	4.6	5.9	2.2
	$Ru_{1.7}$/NdScSi	1.4	2.3	3.0	1.2
	$Ru_{1.5}$/SmScSi	1.9	2.7	3.3	1.5
	$Ru_{1.3}$/GdScSi	1.0	2.2	2.9	0.8
	$Ru_{2.1}$/MgO	0.1	0.2	0.4	0.1
300 °C	$Ru_{1.7}$/LaScSi	0.1	0.7	0.9	0.1
	$Ru_{1.7}$/CeScSi	0.5	0.9	1.1	0.5
	$Ru_{1.3}$/GdScSi	0.0	0.0	0.0	0.0
	$Ru_{2.1}$/MgO	0.0	0.0	0.0	0.0

influence on the catalyst behavior since heterogeneous catalysis mainly involves surface reactions. It is worth noting that previous works reported by Kitano *et al.*[9] or Wu *et al.*[14] about the ammonia synthesis over intermetallic-based catalysts did not report the influence of this parameter (not specified in the experimental part of the corresponding paper).

The effect of catalyst grain size on the performance in NH_3 synthesis at 450 °C (H_2:N_2 = 3; 1–5 bar) was examined by sieving the samples in three different ranges: 250–100, 100–40 and < 40 μm. Figure 1A show that, under similar reaction conditions, the ammonia production rate differs significantly depending on the selected grain size range. As expected, the ammonia rate increases with the decrease in the particle size, whatever the reaction pressure from 1 to 5 bar.

A comparison between the $Ru_{1.7}$/LaScSi sample and the reference $Ru_{2.1}$/MgO catalyst is presented in Figure 1B for experiments performed at 1 bar and 450 °C depending on the selected grain size range. It is clear that the effect of grain size is significantly less pronounced with a divided material like $Ru_{2.1}$/MgO (with a specific surface area of about 21 $m^2 g^{-1}$) compared to intermetallics which develop a very low surface area of 1 $m^2 g^{-1}$ (see experimental part). It also illustrates that the reaction rate over $Ru_{2.1}$/MgO was not limited by the intergranular diffusion. Finally, due to the uncertainty of the grain distribution in the lowest grain size range (< 40 μm), we have further selected the 100–40 μm range for the study (except mentioned otherwise).

The experimental set-up used to evaluate the performance of catalysts allows a continuous and fast monitoring of the NH_3 synthesis reaction as a function of time under controlled temperature and pressure. Our protocol usually includes a first step under $N_2 + H_2$ at 300 °C (1 bar during 1 h) and four consecutive measurements at 400 °C under 1, 3, 5 and 1 bar (1 h each). The results obtained with the $Ru_{1.7}$/LaScSi material are presented in Figure 2A and compared to the reference catalyst $Ru_{2.1}$/MgO. The step at 300 °C (between t = 1.2 h and t = 2.2 h) is carried out in order to evaluate the activities at low

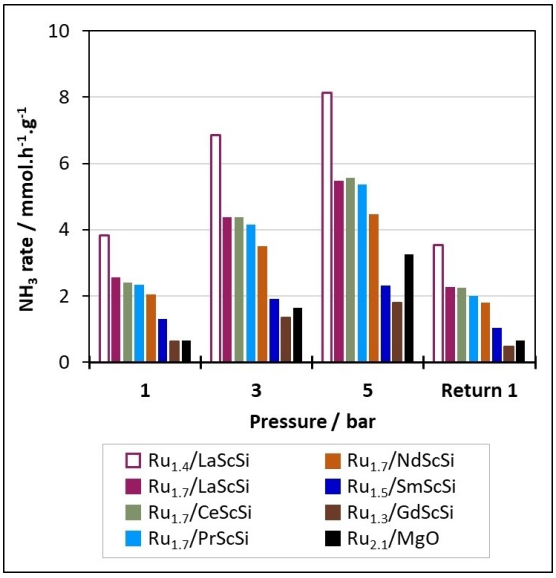

Figure 4. Effect of rare earth (R: La, Ce, Pr, Nd, Sm, Gd) on Ru/RScSi (100-40 μm) catalysts on the NH_3 production rate/*mmol.h^{-1}.g^{-1}* at 400 °C.

temperature but also to promote the hydride formation of the catalysts in the case of intermetallics (this specific point is discussed thereafter in the study). Figure 2A shows that the $Ru_{1.7}$/LaScSi catalyst (purple line) shows an activity at 300 °C with a formation of about 100 ppm of NH_3, which is not observed for the $Ru_{2.1}$/MgO sample (Table 3). The ammonia production is then studied at 400 °C from 1 to 5 bar. Whatever the gas inlet pressure, the intermetallic based catalyst systematically shows higher NH_3 yields than the sample supported on MgO. Moreover, it is also observed that ammonia formation on $Ru_{1.7}$/LaScSi is pressure-dependent since the outlet ammonia concentration is doubled from 1 to 5 bar for $Ru_{1.7}$/LaScSi, from 1710 to 3650 ppm, respectively. For $Ru_{2.1}$/MgO, the amount of ammonia is multiplied by five (from 420 to 2170 ppm) (Table 3). These results are consistent with the work of Wu *et al.*[14] Figure 2A also points out that the ammonia production is not constant over $Ru_{1.7}$/LaScSi during each stage of the test. A decrease with time was observed while the activity of $Ru_{2.1}$/MgO appears more stable.

To study the stability of the Ru/LaScSi sample in ammonia synthesis compared to $Ru_{2.1}$/MgO reference, each sample was submitted to two consecutive catalytic tests under the H_2:N_2 flow (3:1) including the pretreatment at 300 °C (1 bar during 1 h) and four consecutive measurements at 400 °C under 1, 3, 5 and 1 bar (1 h each) before cooling to room temperature under nitrogen (1 h each) before cooling to room temperature under nitrogen (and one night without gas flow). For these experiments, another batch of Ru/LaScSi was used, with 1.4 $_{wt}$% Ru ($Ru_{1.4}$/LaScSi; activities of both catalysts are reported in Figure 4). Results presented in Figure 2B evidence a loss of activity for $Ru_{1.4}$/LaScSi of about 20% between the first run and the second run. In contrast, the reference $Ru_{2.1}$/MgO sample remains stable in similar conditions, but its activity was still significantly lower compared to $Ru_{1.4}$/LaScSi. These results were assigned to a sintering effect of Ru particles revealed by TEM experiments performed over $Ru_{1.4}$/LaScSi (Figure 3). Indeed, the mean size of the ruthenium particles from TEM analysis increases from 5.6 nm to 9.6 nm after two catalytic runs at 400 °C up to 5 bar. These results highlight the aggregation of Ru nanoparticles over the electride support which tends to cause a rapid decay of activity and thus a durability drawback. These observations confirm some previous results reported for Ru/intermetallics dedicated to ammonia synthesis. Indeed, the method of Ru deposition is a key point to obtain strong metal-support interaction in order to avoid Ru particles aggregation and facilitate electron transfer.[10a,19] As the ruthenium deposition method differs between Ru/*R*ScSi samples and Ru/MgO (see experimental part), a specific study about the impact of the ruthenium deposition method on MgO support is reported in Supplementary Information (Figures S2 and S3).

The influence of the rare earth element (*R*) in Ru-supported *R*ScSi electrides for ammonia synthesis is thereafter investigated. The catalytic performance of ruthenium catalysts depends on the loading and thus on the particle size distribution of Ru.[20] Consequently, the effect of the nature of the rare earth on the Haber-Bosch synthesis is compared with close ruthenium contents (1.3–1.7 $_{wt}$%). As previously exposed, the usual catalytic test includes a first step under $N_2 + H_2$ at 300 °C (1 bar during 1 h) and four consecutive measurements at 400 °C under 1, 3, 5 and 1 bar (1 h each). Figure 4 shows the mean NH_3 yields measured at 400 °C between 1 and 5 bar for the Ru supported *R*ScSi-catalyst series sieved in the 100–40 μm range (*R*=La, Ce, Pr, Nd, Sm, Gd). The corresponding mean NH_3 emission (ppm) are reported in Table 3. The results are compared to the $Ru_{2.1}$/MgO reference material. Note that no activity is observed in the absence of ruthenium, whatever the considered support.

With the exception of the $Ru_{1.4}$/LaScSi catalyst which seems to exhibit a different behavior, the materials with a Ru content of 1.7 $_{wt}$% supported on LaScSi, CeScSi and PrScSi show similar activities, with ammonia yields reaching 5.6 $mmol.h^{-1}g^{-1}$ at 5 bar (400 °C). On the opposite, the catalyst based on SmScSi support presents lower activities. Ammonia yields still always increase with pressure but to a limited extent, so that the reference material is more active at high pressure than $Ru_{1.5}$/SmScSi. $Ru_{1.3}$/GdScSi shows lower activities compared to other intermetallics, with limited NH_3 emissions compared to $Ru_{2.1}$/MgO. The poor catalytic activity of the gadolinium containing catalyst is discussed thereafter in this study. Based on ammonia rate (Figure 4), $Ru_{1.7}$/NdScSi sample shows an intermediate behavior. In addition, the two Ru/LaScSi samples with 1.4 $_{wt}$% and 1.7 $_{wt}$% Ru shows significantly different catalytic behaviors. The higher ammonia rate observed for $Ru_{1.4}$/LaScSi (8.1 $mmol.h^{-1}.g^{-1}$ at 5 bar, 400 °C) is attributed to the lower Ru particles size at 5.6 nm compared to 9–18 nm for other samples (Table 2). In fact, it is accepted that the NH_3 synthesis reaction is structure sensitive. For Ru-based catalysts, the B5-type surface sites are reported to be responsible for the activity.[21] These specific surface sites are expected to be favored over Ru crystallites exhibiting diameters in the 3–5 nm range.[22] In addition, Gong *et al.*[10a] recently showed that the transition metal in ternary La-TM-Si intermetallics (TM=Co, Fe, and Mn) intermetallics influences the ruthenium-support interactions.

Then, to overcome the Ru particle size effect and to highlight the impact of electride-hydride properties of Ru supported intermetallics catalyst, the ammonia formation rate is also expressed as turn over frequency (TOF) in Table 4. TOF is calculated as the number of moles of NH_3 emitted per time unit divided by the amount (mol) of surface ruthenium (estimated from the average Ru particle sizes measured by TEM, Figure S1 in the Supplementary Information file). Results presented in Table 4 firstly highlight that intermetallic supports allow significantly higher catalytic performance than the reference MgO materials. This result clearly highlights the specific role of electride-hydride properties and suggests that the intrinsic activity of the Ru catalyst is highly improved by the Ru/intermetallic interaction.

Comparison of data expressed as NH_3 production rate (Figure 4) and TOF (Table 4) shows slight differences. Although the supported LaScSi, CeScSi and PrScSi catalysts remain the most active materials, the Sm-based sample becomes close to NdScSi and GdScSi. Note that the $Ru_{1.3}$/GdScSi remains the less active sample. Regarding the effect of Ru content on LaScSi, the

$Ru_{1.4}$/LaScSi material, which has a higher NH_3 formation rate than $Ru_{1.7}$/LaScSi (Figure 4), shows a lower TOF (Table 4).

This result can be explained by the sensitivity of the NH_3 synthesis reaction to the ruthenium structure. The TOF calculated here do not consider only the Ru particles between 3 and 5 nm (type B5) but the average size of the whole accessible Ru particles.

To highlight the specific activity of Ru supported intermetallics catalysts toward N_2 adsorption/dissociation, a study of $^{14}N_2$/$^{15}N_2$ homomolecular exchange is described below as well as DFT and XRD characterizations.

N_2 activation and hydride characterization

Isothermal $^{14}N_2$/$^{15}N_2$ nitrogen homomolecular isotopic exchange experiments (INHIE: $^{14}N_{2(g)} + {}^{15}N_{2(g)} \rightarrow 2{}^{14}N{}^{15}N_{(g)}$) were undertaken at 450 °C for the studied *R*ScSi-supported Ru catalysts and the $Ru_{2.1}$/MgO reference material. The INHIE reaction is an efficient indicator to evaluate the capacity of the catalyst to adsorb and dissociate the dinitrogen molecule. The dinitrogen profiles recorded with $Ru_{1.7}$/LaScSi and $Ru_{2.1}$/MgO are presented in Figures 5A and 5B, respectively. A pure homomolecular exchange occurs on $Ru_{1.7}$/LaScSi, illustrated by a simultaneous decrease with time in the partial pressure of $^{14}N_2$ and $^{15}N_2$ and a concomitant increase in the partial pressure of $^{14}N^{15}N$. Similar trends are obtained for all intermetallics, but with various kinetics. In comparison, neither a consumption of $^{14}N_2$ and $^{15}N_2$ nor an increase in $^{14}N^{15}N$ signal were observed with $Ru_{2.1}$/MgO at 450 °C. The promotion of the homomolecular exchange reaction on Ru/*R*ScSi samples indicates that the dissociation of N_2 on Ru is favored by intermetallics support compared to the reference $Ru_{2.1}$/MgO material.

This result is in agreement with the reported electride character of intermetallics which are electron-donor materials.[9,14] A comparison of the Ru/*R*ScSi behaviors for N_2 dissociation can be achieved by calculating the initial rate of homomolecular exchange (R_q) from the slope of the m/z = 29 curve at the beginning of the reaction (Eq. 1, experimental part). The results reported in Table 3 show that $Ru_{1.7}$/LaScSi, $Ru_{1.7}$/CeScSi and $Ru_{1.7}$/PrScSi exhibit high equilibrium rates, at 5.54×10^{23} at.g^{-1}.min^{-1}, 5.01×10^{23} at.g^{-1}.min^{-1} and 1.39×10^{23} at.g^{-1}.min^{-1}, respectively. For $Ru_{1.7}$/NdScSi and $Ru_{1.5}$/SmScSi, lower equilibration rates were observed, at $1.52\text{x}10^{22}$ and 0.46×10^{22} at.g^{-1}.min^{-1}, respectively. On $Ru_{1.5}$/SmScSi, for which the equilibration was extremely low at 450 °C, a temperature-programmed analysis of the reaction was performed between 450 °C and 600 °C (Figure S4). This additional experiment shows that a temperature of 580 °C is required to obtain a significant rate of equilibration for this samarium containing sample. Finally, the $Ru_{1.3}$/GdScSi sample exhibits an intermediate behavior with an initial equilibrium rate of 4.42×10^{22} at.g^{-1}.min^{-1} at 450 °C.

The cleavage of the N_2 bond is commonly recognized as the rate-determining step of ammonia synthesis pathway. Consequently, a tentative of correlation between the ammonia yield at 400 °C and the equilibration activity measured at 450 °C is reported in the Figure 6. Interestingly, the Ru/*R*ScSi catalysts with the highest ammonia production rate ($Ru_{1.7}$/LaScSi and $Ru_{1.7}$/CeScSi) also have the highest equilibrium rate, while the catalyst with the lowest ammonia formation rate ($Ru_{1.5}$/SmScSi) shows the lowest N_2 equilibrium rate. However, $Ru_{1.3}$/GdScSi does not follow this correlation with an intermediate N_2 equilibrium rate but a very low ammonia synthesis rate. Additionally, the reference $Ru_{2.1}$/MgO catalyst presents no N_2

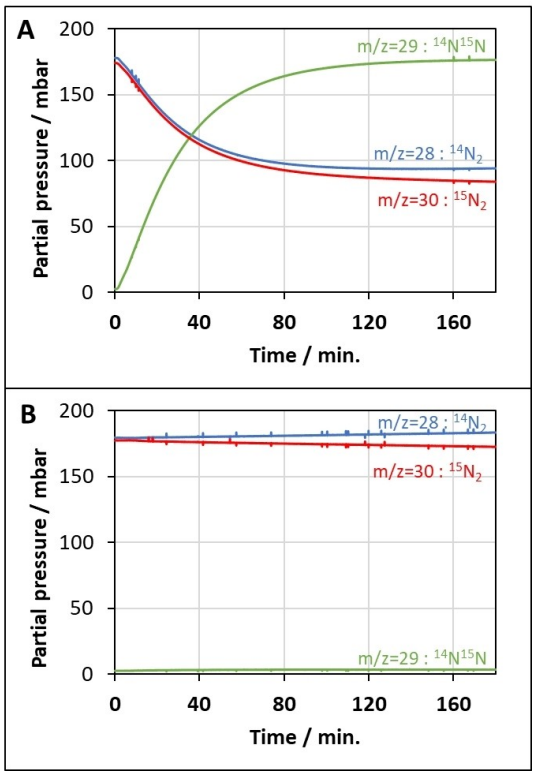

Figure 5. Evolution of the nitrogen isotopomer partial pressures during a homomolecular (INHIE) experiment at 450 °C for A: $Ru_{1.7}$/LaScSi, B: $Ru_{2.1}$/MgO.

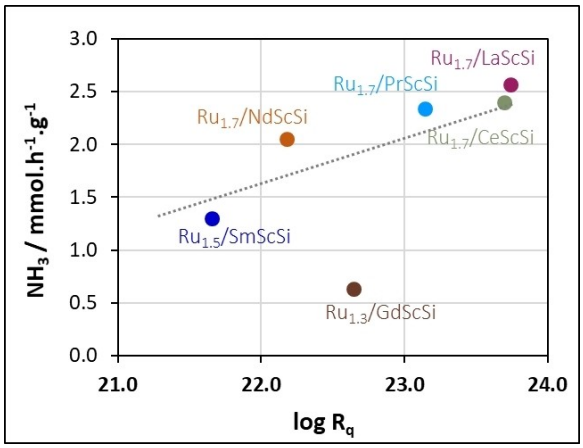

Figure 6. Correlation between the initial rate of equilibration at 450 °C and the ammonia production rate at 400 °C on Ru/RScSi samples. $Ru_{1.7}$/LaScSi ((Text/Zahl)), $Ru_{1.7}$/CeScSi (●), $Ru_{1.7}$/PrScSi (●), $Ru_{1.3}$/GdScSi (●), $Ru_{1.7}$/NdScSi (●) and $Ru_{1.5}$/SmScSi (●).

exchange activity at 450 °C. To go further insight in NH_3 synthesis route, DFT and XRD investigations are described thereafter.

To identify the possible phase changes during the catalytic tests performed at 400 °C, XRD patterns were collected at room temperature after the tests. The diffractograms of Ru/*R*ScSi samples for *R*=La, Nd and Gd are shown in Figure 7 and the unit cell parameters of the phases obtained after catalytic tests are listed in Table 1 for all tested rare earths. From these results, it appears that LaScSi, CeScSi, and PrScSi samples exhibit only one single hydride phase after the catalytic test, while NdScSi and SmScSi show also the formation of a hydride phase but with remaining pristine material. The relative proportion of hydride phase, estimated by Rietveld refinement, decreases from Nd to Sm. Finally, GdScSi does not form any hydride phase and only the pristine intermetallic is present.

Therefore, this firstly evidences that the hydrogenation process differs depending on the rare earth nature and becomes more difficult when going from La to Gd lanthanides.

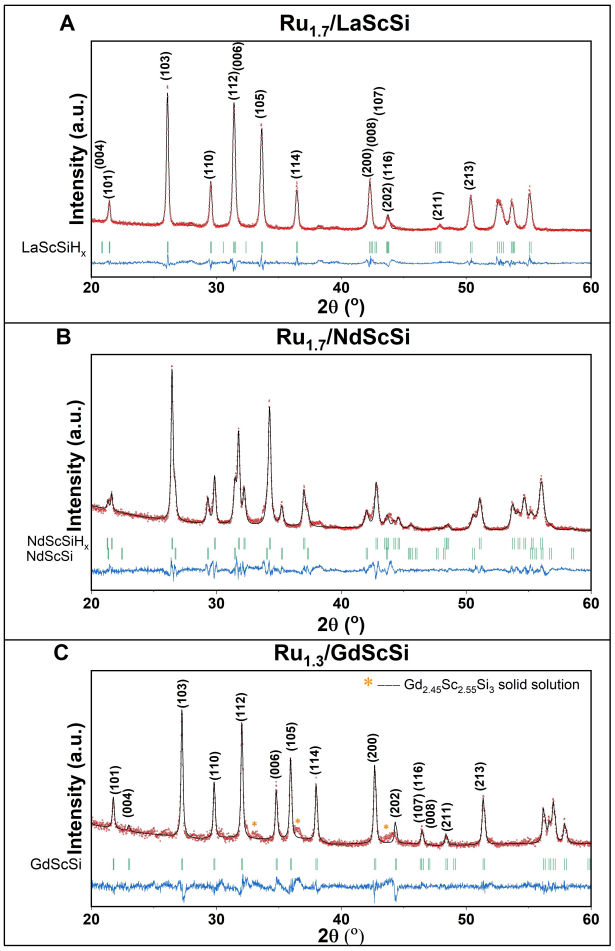

Figure 7. Full pattern matching of XRD patterns obtained after catalytic tests at 400 °C for three different samples (each was tested at 1, 3, and 5 bar). The Bragg peaks positions are marked with ticks and the indexations are given for single-phase samples. The difference curve between calculated and measured curves is shown below (blue curve). (A): $Ru_{1.7}$/LaScSi after catalytic test at 400 °C. (B): $Ru_{1.7}$/NdScSi after catalytic test at 400 °C. (C): $Ru_{1.3}$/GdScSi after catalytic test at 400 °C.

Besides, as the catalytic performances tend to decrease from the lightest rare earths to the heavier ones, it also suggests that the formation of the hydride phase favors the catalytic activity of Ru/*R*ScSi materials, likely by enhancing the electron-donating character of the support.[9] Note that those measurements were performed back to room temperature, meaning that *in-situ* XRD would be required to confirm the hydrogenation state during the catalytic tests. As previously noted, the $Ru_{1.3}$/GdScSi sample exhibits different behavior compared to the other ones (Figure 6). The fact that no correlation is observed between the N_2 exchange and the ammonia production rate needs further experiments and DFT calculations to be understood.

Our previous theoretical works on GdScGe and NdScSi and their hydrides, using density functional theory (DFT), gave insights on the effect of both the nature of the rare earth and the presence of hydrogen, on features closely related to the electride character.[17d,23] The electronic structure of GdScGe and NdScSi was found spin-polarized, which is expected from, at least, the significant magnetic moment from Nd and Gd 4f shells. Sc bands are thus spin-polarized too, especially since Sc and Gd/Nd are first-neighbors. Since the electride charge density arises from the overlap of Sc s and p atomic orbitals,[14] the spin polarization of Sc bands lifts the degeneracy of spin-up and spin-down electride states, thus removing at least half the electride states from the vicinity of Fermi level. Also, the spin polarization induces a charge transfer from the minority spin toward the majority spin channel, likely to depopulate the electride states.

Upon hydrogen insertion in the tetrahedral sites of the rare earth double layers, the spin polarization of Sc bands vanishes, and only 4f-character bands retain a magnetic moment, consistently with the loss of long-range magnetic ordering observed experimentally. This striking effect, due to the strong RE–H interactions competing with RE–Sc interactions, potentially restores the full electride character, as in the non-magnetic LaScSi. However, two conditions are necessary for this electronic structure effect to actually achieve an electride character: i) obviously, the octahedral R_2Sc_4 sites should remain mostly hydrogen-free, since they host the electride charge density. This condition is intrinsically satisfied in GdScGeH ($GdScGeH_{1.5}$ has never been observed); ii) hydrogen insertion goes along with a lowering of Fermi level, potentially depopulating the electride states. Therefore, a second condition is that the electride states remain populated, at the vicinity of Fermi level. Interestingly, GdScGeH meets this condition as well.[17d] From our preliminary calculations (to be published) we assume that GdScSi has a similar behavior.

In conclusion of this DFT part, the 4f-shell magnetic moment perturbs significantly the electronic structure near the Fermi level, and could strongly reduce the contribution of electride states as electron donors in the catalytic process, as observed here (Figure 4), especially for Sm and Gd that carry the most populated 4f shells. Hydrogen insertion potentially solves this issue, and a complete DFT study is ongoing to address these aspects in intermetallics of interest here.

Electride and hydride behaviors in NH_3 synthesis reaction; mechanistic insights

As a result, a specific study on $Ru_{1.7}$/LaScSi and $Ru_{1.7}$/CeScSi catalysts compared to $Ru_{1.3}$/GdScSi and $Ru_{2.1}$/MgO reference was undertaken in the following section to highlight the involvement of electride and hydride behaviors in NH_3 synthesis reaction.

First, the catalytic performances at very low temperature (300 °C) were determined over $Ru_{1.7}$/LaScSi and $Ru_{1.7}$/CeScSi in order to provide further information on the mechanism encountered on these electride samples. For sake of comparison, the $Ru_{1.3}$/GdScSi sample which showed intermediate N_2 equilibration rate (Figure 6) and no hydride behaviors (Figure 7) was also evaluated, as well as the $Ru_{2.1}$/MgO reference catalyst.

Figure 8A shows the performances of the selected materials in ammonia synthesis at 300 °C depending on the pressure. First the $Ru_{1.3}$/GdScSi material and the $Ru_{2.1}$/MgO reference sample present no activity at 300 °C even at 5 bar. To the opposite, the cerium-based catalyst shows remarkable activities with ammonia yield of 1.35 mmol.h^{-1}.g^{-1} (900 ppm) compared to 0.97 mmol.h^{-1}.g^{-1} (650 ppm) for $Ru_{1.7}$/LaScSi at 5 bar. Note that 0.58 mmol.h^{-1}.g^{-1} is reached from 1 bar over $Ru_{1.7}$/CeScSi. The higher ammonia synthesis performances at 300 °C of cerium-based intermetallic is also confirmed by the TOF calculation on Ru particles (Table 4).

H_2-TPD experiments were then carried out to study the hydrogen-sorption properties of intermetallic samples. Note that Ru addition on *R*ScSi has no effect in H_2-TPD curve profiles and that no desorption was observed for the $Ru_{2.1}$/MgO sample (results not shown). Figure 8B shows that very low H_2 desorption was recorded for Gd-based material. This result seems to indicate that the hydride-phase was not formed over GdScSi intermetallic during the adsorption phase performed at 350 °C. This particular behavior for R = Gd might be related to the inability of GdScSi phase to absorb H_2, as previously highlighted by XRD analysis (Figure 7). Despite the electride character of this material, which promotes the transfer of electrons from Ru to the antibonding π-orbitals of N_2 ($^{15}N_2$/$^{14}N_2$ equilibration experiments), the hydrogenation step is limited under the $N_2 + H_2$ reactional mixture. In addition to the strong magnetic moment of Gd which should perturb significantly the electride-type density in the Gd_2Sc_4 site (DFT calculations previously discussed), the low activity of $Ru_{1.3}$/GdScSi could also come from the partial poisoning of the Ru nanoparticles by the chemisorbed -H atoms that cannot migrate inside the interstitial sites of the intermetallic phase sites. Figure 8B also shows that the hydrogen release proceeds in different temperature ranges depending on rare earth elements in *R*ScSi-based sample (*R*=La, Ce).

Both catalysts present two main desorption peaks centered at 380–560 °C and 525–625 °C for $Ru_{1.7}$/CeScSi and $Ru_{1.7}$/LaScSi, respectively. Note that the observation of two desorption peaks is in fair agreement with the existence of two different crystallographic sites able to store hydrogen species in the material, *i.e.* the [R_4] tetragonal site and the [R_2Sc_4] octahedral site corresponding to 1H/f.u. and 0.5 H/f.u., respectively. The relative ratio of both peaks suggests that hydrogen is released from the octahedral cavity first, then from the tetrahedral cavity, in accordance with the fact that the latter is reported to be more stable than the octahedral one.[14]

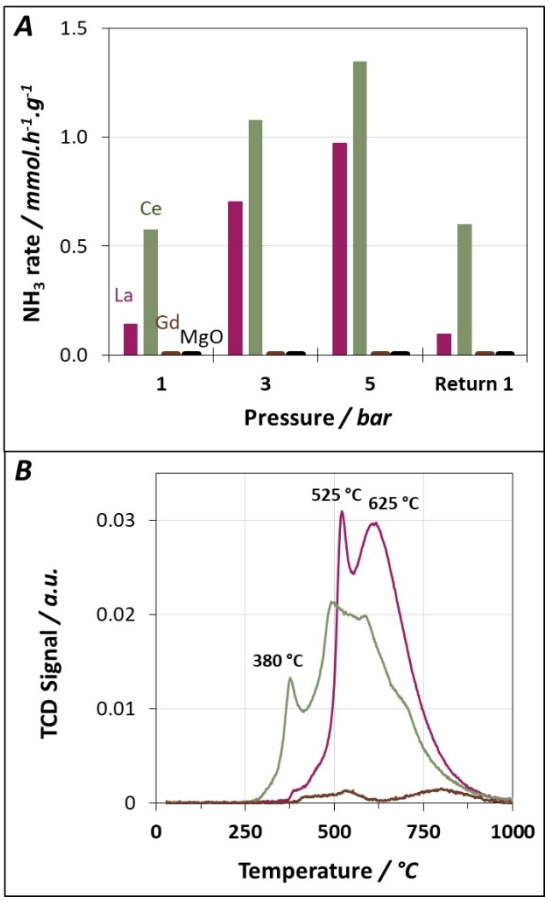

Figure 8. shows the performances of the selected materials in ammonia synthesis at 300 °C depending on the pressure. First the $Ru_{1.3}$/GdScSi material and the $Ru_{2.1}$/MgO reference sample present no activity at 300 °C even at 5 bar. To the opposite, the cerium-based catalyst shows remarkable activities with ammonia yield of 1.35 mmol.h^{-1}.g^{-1} (900 ppm) compared to 0.97 mmol.h^{-1}.g^{-1} (650 ppm) for $Ru_{1.7}$/LaScSi at 5 bar. Note that 0.58 mmol.h^{-1}.g^{-1} is reached from 1 bar over $Ru_{1.7}$/CeScSi. The higher ammonia synthesis performances at 300 °C of cerium-based intermetallic is also confirmed by the TOF calculation on Ru particles (Table 4).

To confirm the hydrogen desorption process, XRD patterns were recorded on $Ru_{1.7}$/LaScSi at three different steps of the desorption curve: (i) after the hydrogen absorption at 350 °C, (ii) after the first desorption peak at 550 °C and (iii) after the complete desorption process up to 1000 °C (Figure 9). The diffractogram obtained before the beginning of the hydrogen release process confirms the presence of the hydride phase $LaScSiH_{1.5}$ with the unit cell parameters a = 4.270 Å and c = 17.072 Å. As expected, the pristine phase LaScSi with higher *a* and much lower *c* values (*a* = 4.348 Å and *c* = 15.984 Å) is recovered after the complete heating up to 1000 °C. After the first H_2-TPD desorption peak, the sample was kept 1 hour at 550 °C and the corresponding diffractogram shows the presence of only one phase with intermediate unit cell parameters

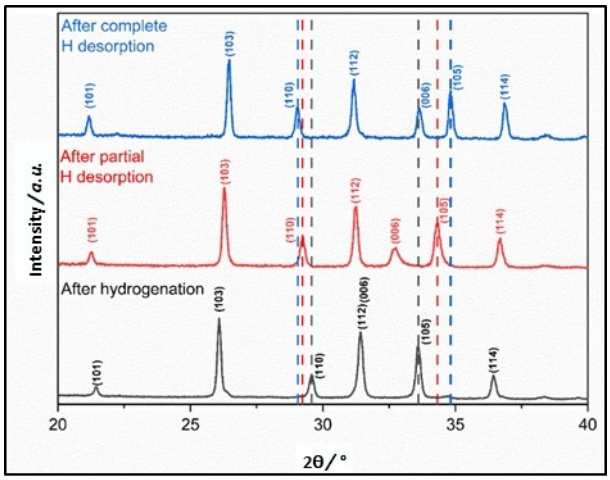

Figure 9. XRD patterns at room temperature after different stages of the H_2-TPD for $Ru_{1.7}$/LaScSi. Below (black): after hydrogenation. Middle (red): after the first desorption peak at 550 °C. Above (blue): after complete desorption up to 1000 °C. The dashed lines emphasize the evolution of the (110) and (105) peaks evidencing the increase of the *a* parameter and the decrease of the *c* parameter upon hydrogen desorption.

($a = 4.319$ Å and $c = 16.400$ Å), evidencing the formation of a partial hydride.

In addition, the difference of activity observed between the two catalysts at 300 °C might be strongly linked to the difference hydride stability observed by H_2-TPD (Figure 8B).

Finally, it appears that the N_2 adsorption/dissociation properties of ruthenium, shown by dinitrogen isotopic exchange experiments (Figure 6), might not be the limiting step in ammonia synthesis for Ru/*R*ScSi samples, and that the H_2 adsorption-desorption properties must be considered as well. In fact, Gong *et al.*[10b] recently proposed a dual-site action mode to explain the activities observed on Ru-loaded La-TM–Si like samples (TM=Co, Fe and Mn) because the rate-determining step was then found to be NH_2 formation. To highlight the mechanisms encountered in NH_3 synthesis over Ru supported LaScSi and CeScSi intermetallic materials, transient catalytic experiments were also carried out.

Two selected Ru/*R*ScSi materials ($Ru_{1.7}$/LaScSi and $Ru_{1.7}$/CeScSi) were evaluated under alternating H_2 (60 mL.min^{-1}) or N_2 (60 mL.min^{-1}) flow at 450 °C. Results of transient catalytic tests are presented in Figure 10.

Over $Ru_{1.7}$/LaScSi, it is clearly evidenced that NH_3 is only emitted under gaseous H_2 flow in absence of N_2 in the gas phase (marked by the green phases), whereas no ammonia is detected under N_2 atmosphere only (marked by the orange phases). These results are consistent with the H_2-TPD profile (Figure 8B) that show rather high stability of the hydride at this temperature, compared to $Ru_{1.7}$/CeScSi. It also shows that N_2 is adsorbed and probably dissociated on the catalyst surface, and that the resulting N species reacted with dissociated H_2 and/or molecular H_2 during the step under pure hydrogen flow. It also emphasizes that NH_3 cannot be emitted without gaseous H_2, meaning that stored H^- species are not able to react with N-

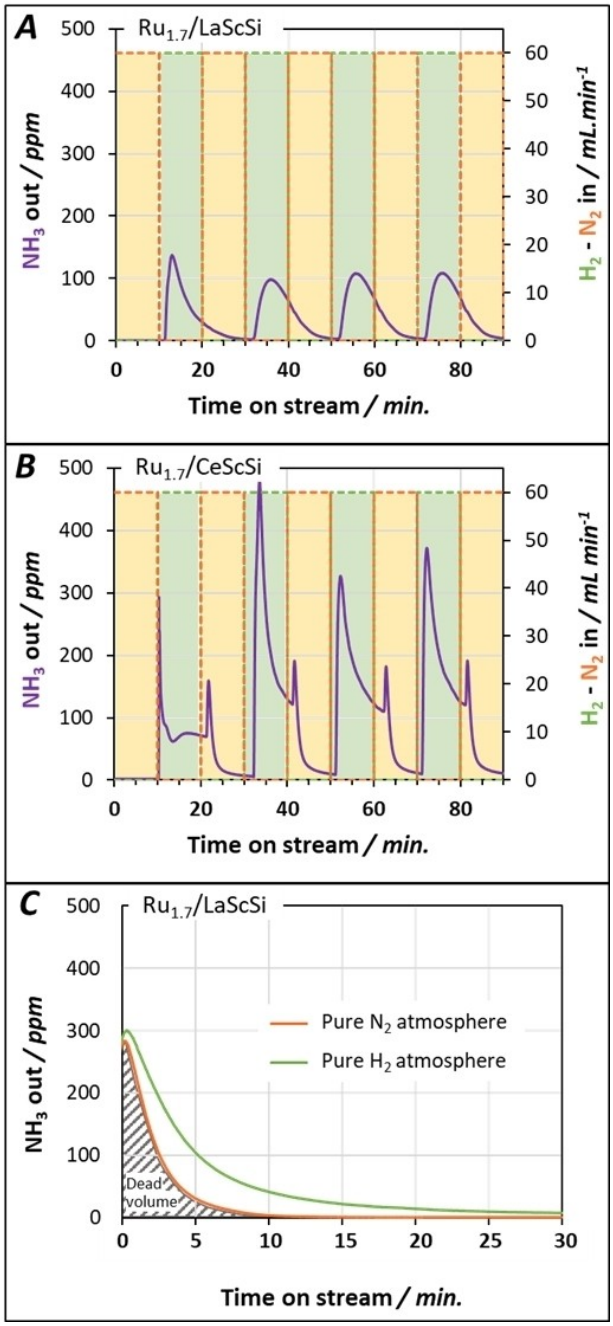

Figure 10. Transient flow experiments with alternative flow of N_2 or H_2 on $Ru_{1.7}$/LaScSi (A) and $Ru_{1.7}$/CeScSi (B) at 450 °C. NH_3 emissions (ppm) at 450 °C under pure N_2 or H_2 purge after NH_3 synthesis on $Ru_{1.7}$/LaScSi (C).

species at this temperature. Concerning the $Ru_{1.7}$/CeScSi catalyst, an ammonia slip is observed during the switch under pure N_2 flow. It is suggested that either (i) adsorbed NH_x-like species remaining on the surface of the material are desorbed during subsequent switch to N_2 or (ii) that cerium-based materials destabilizes hydrogen more efficiently than lanthanum-based ones as indicated by the H_2-TPD results (Figure 8B). The better catalytic performances of the Ce-based compound at 300 °C, while being slightly less efficient at 400 °C compared

with its La-based counterpart, could be then explained by the lower temperature of H desorption of $CeScSiH_X$ hydride. It reveals that hydrogen species as H^- ions may also be involved in NH_3 formation.

Electride-like materials present nanocages containing electrons which can capture hydrogen species as H^- ions. Kitano *et al.*[9] reported that, in $[Ca_{24}Al_{28}O_{64}]^{4+}(e^-)_4$, H^- ions react with nitrogen species formed from N_2 dissociation, which results in ammonia formation. Note that similar behaviors were also encountered over $Ca_2N{:}e^-$ supported Ru catalysts were both electrons and hydride ions likewise play a crucial role in effective ammonia synthesis.[24] The electron-hydride ion exchange reaction by H desorption through a cage wall composed of a rigid monolayer of materials require high temperature to achieve surface metal hydrides. Besides, Wang *et al.*[25] reported that some hydride materials such as the ternary ruthenium complexes Li_4RuH_6 and Ba_2RuH_6 allow the non-dissociative reduction of N_2. It was reported also that hydridic hydrogen transports electrons and proton to stabilize N_XH_Y intermediates. Consequently, hydride desorption temperature impacts the NH_3 production, as illustrated in [11]. Our experiments support that hydride character formed by hydrogen sorption promotes to NH_3 synthesis but ammonia is still mainly formed by reduction of N_2 with hydrogen from the gas phase. Overall, it also supports the dual-site catalytic mechanism concept where the NH_X formation may be considered as the rate-determining step for some kind of catalysts, instead of the generally admitted N_2 adsorption/dissociation step.

These results are confirmed in Figure 10C where the $Ru_{1.7}$/LaScSi catalyst was exposed to pure N_2 or H_2 atmosphere after ammonia synthesis at 450 °C. This experiment confirmed a significant ammonia formation under H_2 while no ammonia emission was observed under N_2 (starting from 400 ppm NH_3, same ammonia purge profiles are obtained without catalyst under N_2 or H_2 flow, denoted as dead volume in Figure 10C). This test highlights again that Ru-supported intermetallic samples can store N-containing species under pure N_2, able to react with gaseous H_2 to produce NH_3. It appears also from Figure 10C that 26 $\mu mol\,g^{-1}$ of stored N_{ad} atom are used at 450 °C over $Ru_{1.7}$/LaScSi sample, compared to 50 $\mu mol\,g^{-1}$ for $Ru_{1.7}$/CeScSi material (curves not shown).

Note that this phenomenon was not observed over $Ru_{2.1}$/MgO catalyst although Szmigel *et al.*[26] revealed by temperature-programmed surface reaction experiments that atomic nitrogen with a surface stoichiometry of $N_{ads}/Ru_s = 1/3$ can be preadsorbed over promoted (Ba, Cs) ruthenium catalysts supported on magnesia.

Conclusion

We have investigated the effect of various rare earth elements on the catalytic activity of Ru supported *R*ScSi silicides (R=La, Ce, Pr, Nd, Sm, Gd) for ammonia synthesis under mild temperature and pressure conditions. A tendency towards a decrease in the catalytic performances is observed when moving from La to Gd, which appears to be related to a lesser ability of the RScSi phases to absorb hydrogen, according to XRD measurements. This could be ascribed to the prevention of hydrogen poisoning of the Ru surface when the hydride phase is formed during ammonia synthesis from H_2 and N_2 gases. In addition, the hydrogen desorption temperature seems to play a role as well in the catalytic activities at low temperature (300 °C). It suggests that the electride character and thus the electron-donor effect can be tuned through partial hydrogenation of the *R*ScSi materials. Further hydrogenation experiments coupled to neutron diffraction study and DFT calculations are under way to better answer this question. Finally, isotopic exchange and transient flow experiments offer a better understanding of the mechanism of ammonia formation. They evidence that the *R*ScSi support helps for the dissociation of the N_2 molecule with possible N- species storage and that hydrogen in the formed NH_3 molecule comes mainly from the gas-phase H_2 and not primarily from the hydride phase. This challenges the involvement of Ru as the only active site and seems to suggest that the formation/desorption of NH_X species could be determinant for NH_3 synthesis performances.

Experimental Section

Materials

The studied *R*TX intermetallic samples are RScSi with R=La, Ce, Pr, Nd, Sm, Gd. They were synthesized from melting the pure elements, starting from rare earth ingots (La 99.9% Sigma-Aldrich, Ce 99.8% Alfa Aesar, Pr 99.9% Smart-elements, Nd 99.9% Smart-elements, Sm 99.9% Alfa Aesar, Gd 99.95% Smart-elements), Sc pieces (99.9% Neyco) and Si lumps (99.9999% Alfa Aesar). Rare earth metals were pre-melted in a high-frequency furnace to evaporate volatile oxides. The molar ratio of 1:1.05:1 with an excess of scandium was used to compensate for residual ScO present in the Sc precursor. The pure metals were cut and weighted to synthesize samples of about 5 g. Then they were arc-melted 5 times under an atmosphere of pure argon (≈700 mbar), returning the button upside down in between each melting to ensure homogeneity. The weight loss of the resulting silvery buttons after melting were less than 0.3 $_{wt}$%. The as-cast samples (i.e. after melting) were later wrapped in tantalum foil, sealed in evacuated quartz ampoules, and annealed at 900 °C for 4 weeks. The method described previously was not used to synthesize SmScSi, as samarium has a high vapor pressure at elevated temperature. Instead, the elements were cut into small pieces and sealed inside a tantalum crucible under argon atmosphere, then they were melted inside a high-frequency induction furnace, and eventually annealed for 10 days at 1000 °C inside a quartz ampoule. As the quality of the samples are comparable, we do not expect any influence of the sample preparation on the catalytic activities.

The resulting pristine buttons were crushed in an agate mortar and sieved in the ranges 250–100, 100–40 and <40 μm for the subsequent deposition of Ru nanoparticles. A theoretical amount of 2.5 $_{wt}$% Ru was used for chemical vapor deposition on the pristine phases using $Ru_3(CO)_{12}$ as Ru precursor in an evacuated quartz tube at 250 °C. This deposition method described in details in ref [9] remains the common technique for intermetallic materials. The starting amount of Ru was chosen after testing of different Ru content (1 to 7.5 $_{wt}$% Ru).

A reference Ru/MgO sample was also prepared for comparison with Ru-supported intermetallic materials. Various processes can be undertaken to prepare conventional ruthenium samples and impregnation is the most commonly used method to obtain Ru-based ammonia synthesis catalysts. MgO support (99.99%, Acros Organic) was first calcinated under air at 500 °C during 2 h (5 °C.min^{-1}). 2.5 $_{wt}$%. Ru was added by impregnation of the corresponding amount of ruthenium nitrosylnitrate solution (Ru-(NO)(NO$_3$)$_3$, Alfa Aesar) in excess of water. The preparation was stirred during 12 h, then dried at 80 °C using a sand bed and placed in an oven at 100 °C during a night. The solid was then treated 2 h at 300 °C under a flow of H_2 (60 mL.min^{-1}, heating ramp rate: 5 °C.min^{-1}). Finally, the sample was sieved between 100 and 40 μm for the catalytic testing. Other sieved ranges have been tested and mentioned when appropriate. The effect of the carbonyl precursor on ruthenium deposition on MgO was also investigated. The results are presented in the supplementary information file.

Characterization

X-ray diffraction. The samples were analyzed after melting, annealing, and catalytic activity test by powder X-ray diffraction (XRD). The data were collected at room temperature (RT) on a PANalitycal X'pert PRO MPD diffractometer in Bragg-Brentano θ-θ geometry equipped with a secondary monochromator and X'Celerator multi-strip detector. Each measurement was made within an angular range of 2θ = 8–80° and lasted for 87 minutes. The Cu–Kα radiation was generated at 45 kV and 40 mA (λ = 1.5418 Å). Powder XRD patterns were analyzed using the Fullprof Suite program and the unit cell parameters were determined through full-pattern matching.[27] Rietveld method was also used to estimate the relative proportion of each phase when both pristine and hydride phases were present in the sample.

Elemental analyses. They were carried out to assess the ruthenium loadings. After solubilisation of the samples in acid media, analyses were performed with an ICP-OES apparatus (Agilent 5110S).

Transmission Electron Microscopy (TEM). Micrographs were recorded on JEOL 2100 instrument operated at 200 kV with a LaB_6 source and equipped with a Gatan Ultra scan camera. EDX spectroscopy was carried out with a Hypernine (Premium) detector (active area: 30 mm^2) using the software SM-JED 2300T for data acquisition and treatment. EDX analysis zone was defined on the particle, and it was generally ranging from 5 to 15 nm. Ru dispersion was averaged over both spherical metal particles and hexagonal close packed particles (*hcp*) model to cover a wide range of particle sizes.[28]

Surface Area and Porosimetry. Nitrogen adsorption-desorption isotherms were recorded at −196 °C, using a Tristar 3000 Micromeritics apparatus. Prior to the measurement, the samples were pretreated at 250 °C under vacuum for 8 h. The surface area was calculated using the BET model. Note that intermetallic-based catalysts present very low specific area of around 1 m^2 g^{-1} compared to 21 m^{2}g^{-1} for $Ru_{2.1}$/MgO reference sample.

Nitrogen isotopic exchange. Experiments were performed in a setup described in [29]. The sample was placed in a U-form quartz reactor and the reaction was carried out in a closed recycle system which was connected to (i) a mass spectrometer (Pfeiffer Vacuum, QMS 200) for the monitoring of the gas phase composition and (ii) to a vacuum pump. The recycling pump placed in the system removes limitations due to gas-phase diffusion. The isothermal nitrogen homomolecular isotopic exchange experiments (INHIE, also called equilibration reaction) were undertaken on 100 mg of catalysts. The sample was treated under pure hydrogen at 350 °C (10 °C.min^{-1}, 1 h) followed by a vacuum step from 350 °C to 450 °C (10 °C.min^{-1}) for 30 min. After the purge, the isotopic mixture was charged (200 mbar of $^{14}N_2$ and 200 mbar of $^{15}N_2$, 98% + purity, supplied by Cambridge Isotope Laboratories, Inc.). The 28, 29, and 30 m/z signals were monitored as a function of time to follow the exchange. The m/z values of 2, 17, 18 and 32 were also recorded to determine the possible releasing of H_2 from the material after hydrogenation, the possible formation of NH_3 during the reaction and the eventual possible leakage causing air entrance in the system. The initial rate of homomolecular exchange (rate of equilibration) is given by Eq.1:

$$R_q(t=0) = \frac{2N_g}{P_0}\left(\frac{dP_{29}}{dt}\right)_{t=0} \quad (1)$$

Where N_g is the number of ^{15}N and ^{14}N in the gas phase; P_0 the total pressure; P_{29} the partial pressure of $^{14}N^{15}N$ and t the time of equilibration.

H_2-TPD (temperature programmed desorption). The experiments were performed on a Micromeritics Autochem 2920 apparatus equipped with a thermal conductivity detector (TCD). Catalyst (50 mg) was placed in a U-shape quartz reactor. Before the measurement, catalysts were first treated under pure hydrogen from RT to 350 °C (5 °C.min^{-1}) and cooled down to RT under H_2, followed by purging step under argon for 1 hour. Note that similar TPD results are obtained with a purge step at 100 °C. Next, temperature programmed desorption is carried out up to 1000 °C (5 °C.min^{-1}) under 30 mL.min^{-1} of Ar.

Catalytic tests

The ammonia synthesis activity measurement was carried out in a fixed-bed reactor under a flow of H_2:N_2 (3:1) (N_2 > 99.9999% and H_2 > 99.9999%). The catalyst (100 mg) was placed in a home-made pressure reactor and the total flow rate was fixed at 60 mL min^{-1}. The gas mixture was imposed by electronic mass-flow controllers.

The compositions of the feed gas and effluent stream were monitored continuously (1 Hz) using online MKS 2030 Multigas infrared analyzer with high NH_3 sensitivity (2-3 ppm). Ammonia synthesis was recorded from RT to the desired temperature (heating ramp of 5 °C min^{-1}). Isotherm experiments were carried out to evaluate the stability of catalysts and the pressure effect up to 5 bar, using a back-pressure regulator. Results are expressed directly in term of emitted ammonia (ppm), synthesis rate (mmol/h/g) or turn over frequency (TOF, min^{-1}) estimated from the average Ru particle sizes measured by TEM.

Transient experiments were performed at stabilized temperature after an increase to the desired temperature under N_2 flow. The catalyst was then submitted to an alternating atmosphere of pure hydrogen or nitrogen every 10 min with a total flow of 60 mL.min^{-1}.

Acknowledgements

The authors gratefully acknowledge the French National Agency for Research (ANR, Intermetalyst Project, ref. ANR-19-CE07-0023), the Regional Council of Nouvelle Aquitaine, the French Ministry of Research and the European Regional Development Fund (ERDF) for financial supports.

Conflict of Interest

The authors declare no conflict of interest.

Data Availability Statement

The data that support the findings of this study are available from the corresponding author upon reasonable request.

Keywords: intermetallic · hydride · NH_3 · ruthenium · transient experiments

[1] H. Liu, *Chin. J. Catal.* **2014**, *35*, 1619–1640.
[2] A. Afif, N. Radenahmad, Q. Cheok, S. Shams, J. H. Kim, A. K. Azad, *Renewable Sustainable Energy Rev.* **2016**, *60*, 822–835.
[3] R. Javaid, H. Matsumoto, T. Nanba, *ChemistrySelect* **2019**, *4(7)*, 2218–2224.
[4] G. Ertl, *Angew. Chem. Int. Ed. Engl.* **1990**, *29*, 1219–1227.
[5] a) B. C. McClaine, R. J. Davis, *J. Catal.* **2002**, *211*, 379–386; b) Y. V. Larichev, B. L. Moroz, V. I. Zaikovskii, S. M. Yunusov, E. S. Kalyuzhnaya, V. B. Shur, *J. Phys. Chem. C* **2007**, *111*, 9427–9436; c) N. Saadatjou, A. Jafari, S. Sahebdelfar, *Chem. Eng. Commun.* **2015**, *202*, 420–448.
[6] a) J. S. J. Hargreaves, *Appl. Petrochem. Res.* **2014**, *4*, 3–10; b) N. Bion, F. Can, J. Cook, J. S. J. Hargreaves, A. L. Hector, W. Levason, A. R. McFarlane, M. Richard, K. Sardar, *Appl. Catal. A* **2015**, *504*, 44–50; c) P. Wang, F. Chang, W. Gao, J. Guo, G. Wu, T. He, P. Chen, *Nat. Chem.* **2017**, *9*, 64–70; d) Y. Inoue, M. Kitano, K. Kishida, H. Abe, Y. Niwa, M. Sasase, Y. Fujita, H. Ishikawa, T. Yokoyama, M. Hara, H. Hosono, *ACS Catal.* **2016**, *6*, 7577–7584; e) V. S. Marakatti, E. M. Gaigneaux, *ChemCatChem* **2020**, *12*(23), 5838–5857.
[7] J. L. Dye, *Acc. Chem. Res.* **2009**, *42*, 1564–1572.
[8] S. Matsuishi, Y. Toda, M. Miyakawa, K. Hayashi, T/ Kamiya, M. Hirano, I. Tanaka, H. Hosono, *Science* **2003**, *301*, 626–629.
[9] M. Kitano, Y. Inoue, Y. Yamazaki, F. Hayashi, S. Kanbara, S. Matsuishi, T. Yokoyama, S.-W. Kim, M. Hara, H. Hosono, *Nat. Chem.* **2012**, *4*, 934–940.
[10] a) Y. Gong, J. Wu, M. Kitano, J. Wang, T.-N Ye, J. Li, Y. Kobayashi, K. Kishida, H. Abe, Y. Niwa, H. Yang, T. Tada, H. Hosono, *Nat. Catal.* **2018**, *1*, 178–185; b) Y. Gong, H. Li, J. Wu, X. Song, X. Yang, X. Bao, X. Han, M. Kitano, J. Wang, H. Hosono, *J. Am. Chem. Soc.* **2022**, *144*, 8683–8692.
[11] Y. Gong, H. Li, C. Li, X. Yang, J. Wang, H. Hosono, *Chem. Mater.* **2022**, *34(4)*, 1677–1685.
[12] H. Mizoguchi, S.-W. Park, K. Kishida, M. Kitano, J. Kim, M. Sasase, T. Honda, K. Ikeda, T. Otomo, H. Hosono, *J. Am. Chem. Soc.* **2019**, *141*(8), 3376–3379.
[13] Y. Lu, T. Tada, Y. Toda, S. Ueda, T. Yokoyama, M. Kitano, H. Hosono, *J. Am. Chem. Soc.* **2016**, *138(12)*, 3970–3973.
[14] J. Wu, Y. Gong, T. Inoshia, D. C. Fredrickson, J. Wang, Y. Lu, M. Kitano, H. Hosono, *Adv. Mater.* **2017**, *29*, 1700924.
[15] a) S. Gupta, K. G. Suresh, *J. Alloys Compd.* **2015**, *618*, 562–606; b) A. V. Morozkin, L. M. Viting, I. A. Sviridov, I. A. Tskhadadze, J . *Alloys Comp.* **2000**, *297*, 168–175.
[16] a) K. Ooya, J. Li, K. Fukui, S. Iimura, T. Nakao, K. Ogasawara, M. Sasase, H. Abe, Y. Niwa, M. Kitano, H. Hosono, *Adv. Energy Mater.* **2021**, *11*, 2003723; b) J. Kammert, J. Moon, Y. Cheng, L. Daemen, S. Irle, V. Fung, J. Liu, K. Page, X. Ma, V. Phaneuf, J. Tong, A. J. Ramirez-Cuesta, Z. Wu, *J. Am. Chem. Soc.* **2020**, *142(16)*, 7655–7667.
[17] a) E. Gaudin, S. F. Matar, R. Pöttgen, M. Eul, B. Chevalier, *Inorg. Chem.* **2011**, *50(21)*, 11046–11054; b) S. Tencé, T. Mahon, E. Gaudin, B. Chevalier, J. L. Bobet, R. Flacau, B. Heying, U. C. Rodewald, R. Pöttgen, *J. Solid State Chem.* **2016**, *242*, 168–174; c) B. Chevalier, W. Hermes, B. Heying, U. C. Rodewald, A. Hammerschmidt, S. F. Matar, E. Gaudin, R. Pöttgen, *Chem. Mater.* **2010**, *22*, 5013–5021; d) T. Mahon, E. Gaudin, A. Villesuzanne, R. Decourt, J.-L. Bobet, O. Isnard, B. Chevalier, S. Tencé, *Inorg. Chem.* **2018**, *57*, 14230–14239.
[18] Y. Gong, H. Li, C. Li, X. Bao, H. Hosono, J. Wang, *J. Adv. Ceram.* **2022**, *11(9)*, doi.org/10.1007/s40145-022-0633-z.
[19] J. Wu, J. Li, Y. Gong, M. Kitano, T. Inoshita, H. Hosono, *Angew. Chem. Int. Ed.* **2019**, *58*, 825–829; *Angew. Chem.* **2019**, *131*, 835–839.
[20] N. Saadatjou, A. Jafari, S. Sahebdelfar, *Chem. Eng. Commun.* **2014**, 420–448.
[21] C. J. H. Jacobsen, S. Dahl, P. L. Hansen, E. Törnqvist, L. Jensen, H. Topsøe, D. V. Prip, P. B. Møenshaug, I. Chorkendorff, *J. Mol. Catal.* **2000**, *163*, 19–26.
[22] F. R. Garciá-Garciá, A. Guerrero-Ruiz, *Top. Catal.* **2009**, *52*, 758–764.
[23] T. Mahon, E. Gaudin, A. Villesuzanne, B. Chevalier, S. Tencé, *Inorg. Chem.* **2019**, *58*, 15255–15268.
[24] M. Kitano, Y. Inoue, H. Ishikawa, K. Yamagata, T. Nakao, T. Tada, S. Mattsuishi, T. Yokoyama, M. Hara, H. Hosono, *Chem. Sci.* **2016**, *7*, 4036–4043.
[25] Q. Wang, J. Pan, J. Guo, H. A. Hansen, H. Xie, L. Jiang, L. Hua, H. Li, Y. Guan, P. Wang, W. Gao, L. Liu, H. Cao, Z. Xiong, T. Vegge, P. Chen, *Nat. Catal.* **2021**, *4*, 959–967.
[26] D. Szmigiel, H. Bielawa, M. Kurtz, O. Hinrichsen, M. Muler, W. Raróg, S. Jodzis, Z. Kowalcyk, L. Znak, J. Zieliński, *J. Catal.* **2002**, *205*, 205–212.
[27] J. Rodríguez-Carvajal, *Phys. B. Condens. Matter.* **1993**, *192(1–2)*, 55–69.
[28] a) Y. Zhou, Y. Ma, G. Lan, H. Tang, W. Han, H. Li, Y. Li, *Chin. J. Catal.* **2019**, *40*, 114–123; b) A. Comas-Vives, K. Furman, D. Gajan, M. C. Akatay, A. Lesage, F. H. Ribeiro, C. Copéret, *Phys. Chem. Chem. Phys.* **2016**, *18*, 1969–1979.
[29] S. M. Hunter, D. H. Gregory, J. S. J. Hargreaves, M. Richard, D. Duprez, N. Bion, *ACS Catal.* **2013**, *3*, 1719–1725.

Manuscript received: September 28, 2022
Revised manuscript received: December 8, 2022
Accepted manuscript online: December 16, 2022
Version of record online: January 9, 2023